Geomechanics and Engineering, *Vol. 21, No. 3 (2020) 259-268*
DOI: https://doi.org/10.12989/gae.2020.21.3.259

Scale effect of mechanical properties of jointed rock mass: A numerical study based on particle flow code

Xiao Wang[1], Wei Yuan*[1], Yatao Yan[1] and Xue Zhang[2]

[1]*School of Civil Engineering, Southeast University, Nanjing 210096, China*
[2]*College of Mining and Safety Engineering, Shandong University of Science and Technology, Qingdao 266590, China*

(Received February 12, 2020, Revised March 15, 2020, Accepted March 17, 2020)

Abstract. The synthetic rock mass (SRM) were used to investigate the influence of specimen size on the mechanical properties of jointed rock mass. The SRM were established based on parallel bond model (PBM) and smooth joint model (SJM) and the scaled rock specimens were sampled in two SRMs considering three sampling locations. The research results show that the smaller the initial fracture density is, the greater the uniaxial compressive strength (UCS), elastic modulus (E) is when compared with the same sampling location. The mechanical properties of rock specimens obtained by different sampling methods in different SRMs have different scale effects. The strength of rock specimens with more new cracks is not necessarily less than that of rock specimens with fewer new cracks and the failure of rock is caused by the formation of macro-fracture surface.

Keywords: synthetic rock mass; scale effect; mechanical properties; failure mode

1. Introduction

There are a large number of joints, cracks and other structural planes in natural rock mass and these structural planes result in the complex mechanical properties of rock mass. The strength of rock mass is mainly determined by the distribution characteristics and mechanical properties of joints. Rock mass with more weak joints is liable to induce engineering geological hazards. Therefore, it is of great engineering significance to study the mechanical properties of jointed rock mass.

Many scholars have studied the mechanical properties of rock mass in many ways, including laboratory test, in-situ test and numerical simulation. Results of laboratory model studies on rock or rock-like materials showed that different materials and fracture distribution mode of rock mass may cause different failure modes and the mechanical properties of jointed rock mass are different (Wong and Chau 1998, Lee and Jeon 2011, Shemirani *et al.* 2017). The numerical simulation of rock mass based on finite element method (FEM) and discrete element method (DEM) also presented that the failure modes and mechanical properties of jointed rock mass have great discreteness (Toraño *et al.* 2002; Morris *et al.* 2006, Bahaaddini *et al.* 2013, Wang and Tian 2018, Wu *et al.* 2020). Some in-situ tests have been performed to study the mechanical strength characteristics and various methods were provided to estimate the strength, deformation modulus or damage of rock mass (Singh and Rao 2005, Kim *et al.* 2019). These studies have played an important role in promoting the safety and stability of jointed rock mass engineering.

The mechanical properties of rock mass are scale dependent and most studies showed that the mechanical properties of rock mass decrease with the increase of rock scale (Song *et al.* 2018). However, some researches have been reported in the literature that do not follow this trend. For example, the research conducted by Symons (1970), and Bahrani and Kaiser (2016) showed that the trend of the change of the strength of rock mass with increasing specimen size is not clear. The research result of Xi *et al.* (2018) showed that the strength will decrease firstly and then increase with the increasing of rock specimen scales. Therefore, it is necessary to further research the scale effect of mechanical properties of rock mass in order to well understand the mechanism of rock mass instability.

Based on the above researches, this paper considering different rock geological structures and sampling methods, the scale effect of jointed rock mass was studied based on PFC numerical software. The synthetic rock mass (SRM) based on parallel bond model (PBM) and smooth joint model (SJM) were established firstly, and two SRMs with different fracture densities were synthesized. Then three sampling methods were set up to take specimens from SRMs, and uniaxial compression tests were carried out on these specimens. Finally, the influence of scale effect on uniaxial compressive strength (UCS), elastic modulus (E), and failure modes of jointed rock specimens with different sampling location in different SRMs were analyzed. The research results are helpful to further understand the failure mechanism of rock mass.

2. Mechanism of synthetic rock mass (SRM)

Rock masses are complex systems composed of a rock

*Corresponding author, Ph.D. Student
E-mail: yuanw_c@seu.edu.cn

ISSN: 2005-307X (Print), 2092-6219 (Online)

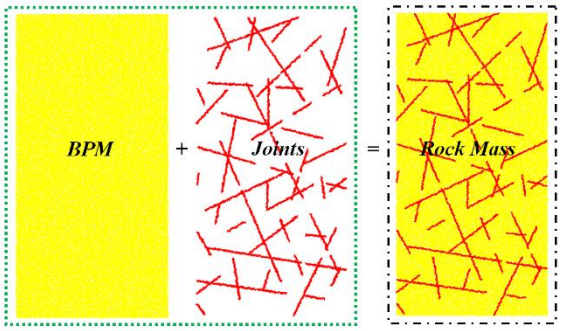

Fig. 1 Mechanism of synthetic rock mass

matrix that may have heterogeneous material properties, often riddled with discontinuities (e.g., fractures, joints, faults, etc.). Failure in such systems may occur in the matrix, along discontinuities at both locations. PFC has been successfully used to study the mechanical behavior of such systems due to the development of the smooth joint contact model. The modeling approach consists of superimposing fracture information (i.e., fracture geometries and properties) onto a bonded particle model (BPM) (Potyondy 2015), as shown in Fig. 1.

2.1 Bonded particle model

There are two kinds of modes of the bonds, named contact bond (CB) and parallel bond (PB), as shown in Fig. 2 (Itasca Consulting Group Inc 2014). The contact bond model provides the behavior of an infinitesimal, linear elastic and either bonded or frictional interface that carries a force (Fig. 2(a)). Because contact bond is point contact, it can only transfer force, but not force moment. When the tensile or shear stress between particles exceeds the normal or tangential bonding strength, the spring will break and the bonding will lose its function. The contact bond model is generally suitable for simulating soil materials.

The parallel bond model regards the bonding between particles as a set of parallel springs, which has the effects of tension, shear and moment, so it can effectively simulate the bonding between particles in rock. In this model, besides the stiffness provided by the bonding spring, the contact spring also provides the stiffness. Once the bonding between particles occurs tension or shear failure, the bonding stiffness will immediately fail, while the contact stiffness still plays a role. When the bond tensile stress or shear stress first exceeds the bond normal strength or tangential strength, the tensile and shear fracture represented by the middle and short lines in Fig. 2(b) occurs in parallel bonding. When a large number of micro-fractures occur between particles, macro-visible cracks are formed. Parallel bonding model is suitable for simulating the mechanical properties of materials such as rock because of its tensile, shear and moment effects and bond failure-deterioration of macro-stiffness.

2.2 Discrete fracture network (DFN)

In PFC^{2D}, the main geometric characteristics of fractures and joints include the direction and trace length. Smooth

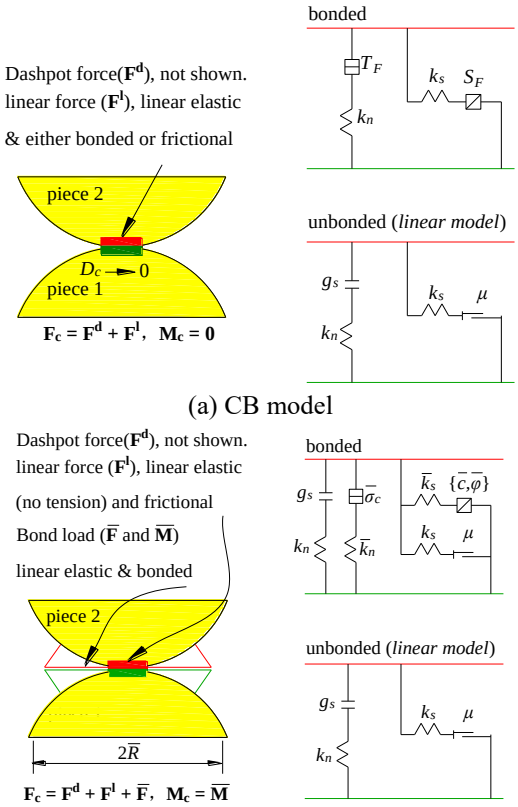

Fig. 2 Bonded-particle model and its micro-mechanical behavior (Itasca Consulting Group Inc. 2014)

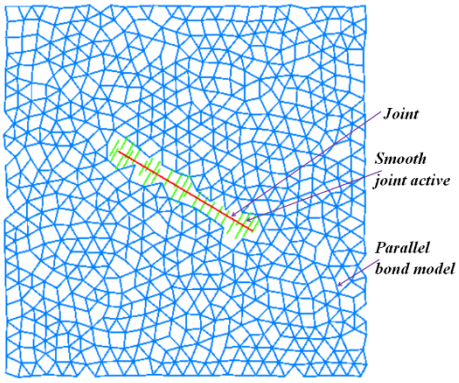

Fig. 3 Discrete fracture network

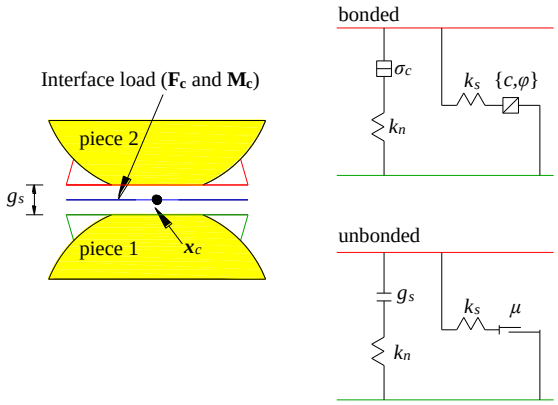

Fig. 4 Behavior and rheological components of the smooth joint model (Itasca Consulting Group Inc. 2014)

joint model is used in discrete fracture network and the parallel bond model intersecting with the network is replaced by smooth-joint contact model when the discrete fracture network is embedded in the particles, as shown in Fig. 3. The smooth joint model simulates the behavior of a planar interface with dilation regardless of the local particle contact orientations along the interface. The behavior of a frictional or bonded joint can be modeled by assigning smooth-joint models to all contacts between particles that lie on opposite sides of the joint. The smooth-joint model provides the macroscopic behavior of a linear elastic and either bonded or frictional interface with dilation. The behavior of the bonded interface is linear elastic until the strength limit is exceeded and the bond breaks, making the interface unbonded; the behavior of an unbonded interface is linear elastic and frictional with dilation, with slip accommodated by imposing a Coulomb limit on the shear force. The interface does not resist relative rotation ($M_c \equiv 0$), as shown in Fig. 4.

There are two methods to generate discrete fracture networks in PFC 5.0. The first method is to generate discrete fracture networks by using distribution functions (such as gauss, lognormal, power-law, uniform, etc.). The second method is to add joints to the network one by one. In this paper, the first method (power-law distribution function) is used to generate discrete fracture network.

3. Synthetic rock mass model and test sample acquisition scheme

3.1 Synthetic rock mass model

Based on the method described in section 2, this section first established a complete rock model based on the PB model, and then inserted the discrete fracture networks into the particle model. Because the main purpose of this paper is to study the mechanical properties of jointed rock mass with different scales, which are 50 mm×100 mm, 75 mm × 150 mm, 100 mm × 200 mm, 125 mm × 250 mm and 150 mm × 300 mm, respectively, a scale of 300 mm × 300 mm of the rock mass model can meet the sampling requirements. Due to the limitation of laboratory test condition, the parameters provided by Zhang *et al.* (2018) were used in parallel bonding model, as shown in table 1.

The discrete fracture networks were generated by power-law distribution function. In this function, the fracture size density distribution defines the number of fracture per unit of area, $n(l)$, whose size is in the range [l; l+dl], is expressed as

$$n(l) = \alpha \cdot l^{-a} \tag{1}$$

where a is the scaling exponent and α is the density term of the DFN model. The distribution is between l_{min} and l_{max} (the lower and upper bounds of the fractures sizes, respectively). a precisely fixes, at any scale, the ratio between (smaller and larger) fracture sizes. It usually in the range from 3 to 4 and when a increases, the proportion of small fractures vs. large fractures increases (Itasca Consulting Group Inc. 2014). The term α fixes the total fracture density by range of fracture size. The total fracture density is additionally dependent on the range of fracture sizes considered with a given DFN model.

If the DFN model is a square domain, L is the side of the square. The number of fractures with size between l_1 and l_2 is given by

$$n(l_1 \le l \le l_2) = \int_{l_1}^{l_2} n(l) \cdot L^2 dl = \alpha \left(\frac{l_2^{1-a} - l_1^{1-a}}{1-a} \cdot L^2 \right) \tag{2}$$

The cumulative fracture size density distribution that defines the number of fractures whose size is larger than a given value $C(l)$ is defined by

$$C(l) = \int_l^{\infty} n(l') \cdot dl' = \alpha \left(\frac{l^{1-a}}{a-1} \right) \tag{3}$$

In order to explore the scale effect of rocks under different geological conditions, two different discrete fracture networks (different fracture density) were set up, as shown in Table 2 and Fig. 5. Because it is difficult to obtain the mechanical and geometric parameters of actual joints, the bond properties of joints are set to 5% of the bond properties of particles (intact rock) by using the experience of Wang *et al.* (2017), and the mechanical properties of joints in different parts of rock mass are assumed to be the same. The mechanical parameters of DFN are listed in Table 3.

3.2 Rock sampling and testing

Because of the different distribution of joints and

Table 1 Physico-mechanical parameters of BPM

Parameter	Value	Parameter	Value
Minimum particle diameter (mm)	0.4	Porosity	0.1
Particle diameter ratio	1.5	Parallel bond friction angle (°)	38
Density (kg/m^3)	2440	Parallel bond tensile strength (MPa)	27.8
Contact modulus of the particle (GPa)	4.0	Normal critical damping ratio	0.5
Parallel bond Deformation modulus (GPa)	27	Parallel bond Cohesive force (MPa)	39
Contact bond gap (mm)	0.05	Stiffness ratio	1.0

Table 2 Parameters of different discrete fracture networks

Schemes	a	α	l_{min}	l_{max}
1	3	0.1	5 mm	300 mm
2	3	0.2	5 mm	300 mm

Table 3 Physico-mechanical parameters of DFN

Parameter	Value	Parameter	Value
Joint tensile strength (MPa)	1.39	Joint normal stiffness (GPa/m)	10
Joint cohesive force (MPa)	1.95	Joint tangential stiffness (GPa/m)	10
Joint friction coefficient	0.7	Joint width (mm)	1

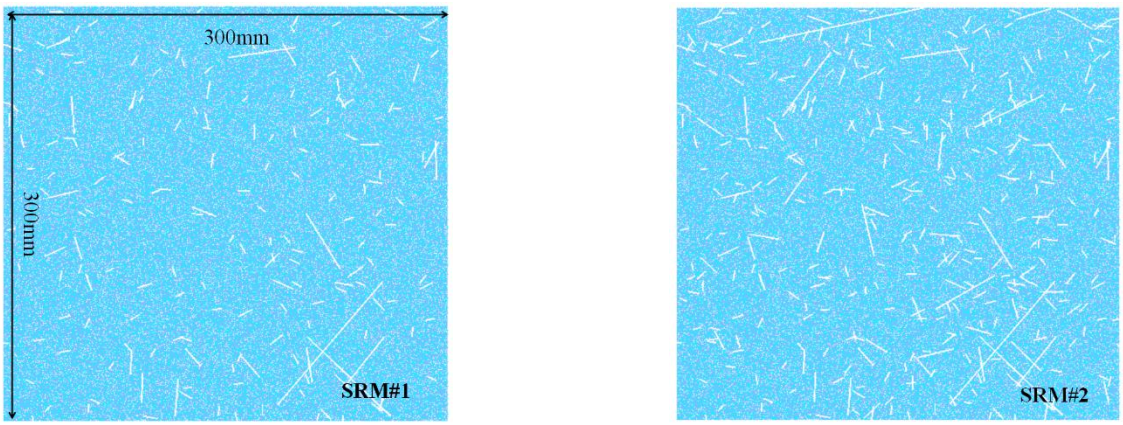

Scheme #1 Scheme #2

Fig. 5 Two discrete networks of synthetic rock mass

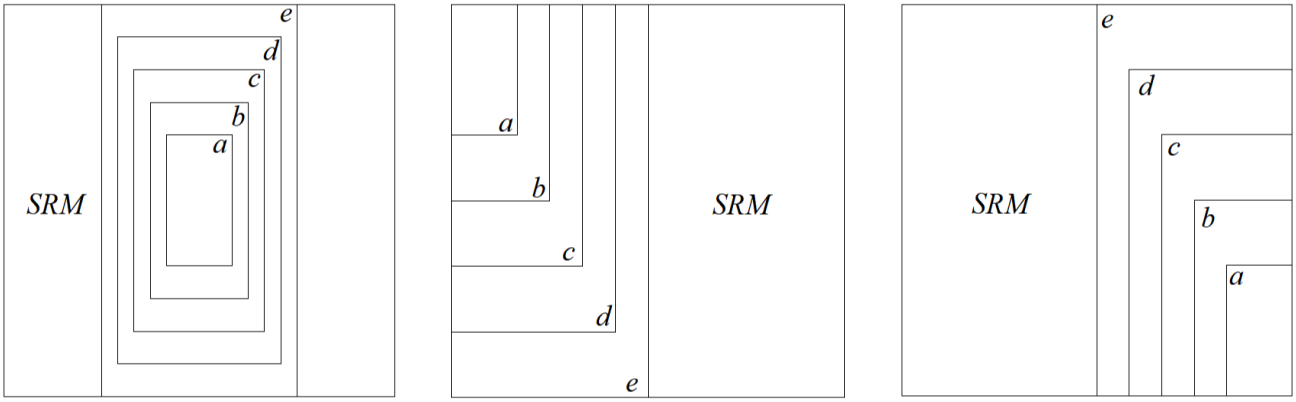

(a) Method A (b) Method B (c) Method C

Fig. 6 Different sampling methods. The size of SRM is 300 mm×300 mm and the sizes of specimen a, b, c, d, e are 50 mm×100 mm, 75 mm × 150 mm, 100 mm × 200 mm, 125 mm × 250 mm and 150 mm × 300 mm, respectively

fissures, different sampling positions of rocks may lead to different mechanics of rocks. Therefore, in order to better illustrate the scale effect of rock mechanical properties, three sampling methods are adopted to obtain the rock samples required for section 3.1, as shown in Fig. 6. The sampling process includes two parts: first, determine the sampling method and sampling location; second, divide the required model area into a group by FISH language and then delete the particles and cracks outside the group.

After the rock sample is taken out, its mechanical properties need to be tested. In PFC, there are two ways to apply loads on rock samples, one is stress mode and the other is displacement mode. For displacement mode loading, it is realized by apply velocity on particles or walls at the top of the model. However, the stress loading mode can only be realized by applying stress on the particles at the top of the model. When the particles are used to load, due to the different size of particles and the gap between particles, the applied stress or displacement will be uneven, resulting in the test results different from the indoor test. Therefore, in this paper, the displacement loading mode controlled by wall is used for uniaxial compression test to analyze the scale effect of mechanical properties of jointed rock samples. The same loading strain rate, 1/s, was used for model loading.

4. Scale effect on mechanical properties of jointed rock specimens

4.1 Mechanical properties of standard rock specimens

Figs. 7 and 8 present the stress-strain curves, uniaxial compressive strength (UCS) and elastic modulus (E) of standard-scale (50 mm×100 mm) rock specimen with different sampling methods in two SRMs. In these figures, the # 1, # 2-represent different SRMs; A, B, C-represent different sampling methods; a-represents standard rock specimens. For instance, #1_Aa represents the standard scale rock specimen (a) taken from the first synthetic rock mass (SRM#1) using the sampling method A. The UCS and E of SRM #1 are larger than SRM #2 compared with the same sampling location (e.g., the UCS and E of rock specimen used method A sampling in SRM #1 are 32.79 MPa and 12.74 GPa, while sampling in SRM #2 are 16.17 MPa and 7.95 GPa). The reason is that the initial crack density of synthetic rock mass #2 is twice that of synthetic rock mass 1, which has larger initial damage and is more likely to lead to crack propagation and penetration, leading to strength failure.

The UCS and E of rock specimens with different sampling method (A, B, C) in same SRM (#1 or #2) are

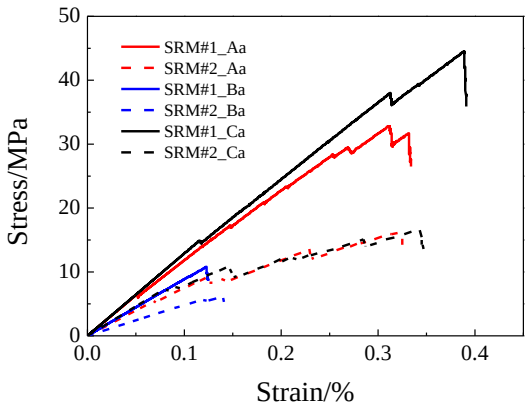

Fig. 7 Stress-strain curves of standard-scale (50 mm × 100 mm) rock specimen with different sampling methods in two SRMs. The # 1, # 2-represent different SRMs; A, B, C-represent different sampling methods; a-represents standard rock specimens. e.g., SRM#1_Aa represents the standard scale rock specimen taken from the first synthetic rock mass using the sampling method A

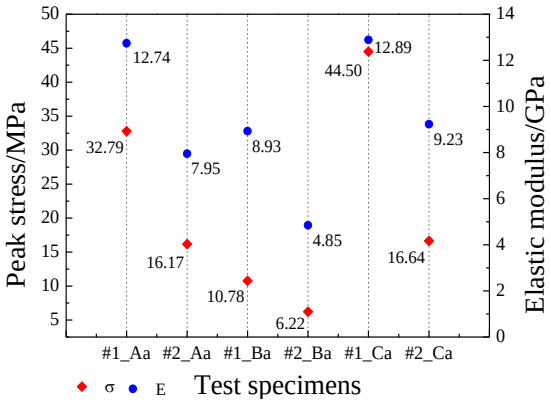

Fig. 8 UCS and E of standard-scale rock specimen with different sampling methods in two SRMs. The UCS represents uniaxial compressive strength and E represents the elastic modulus of rock specimens

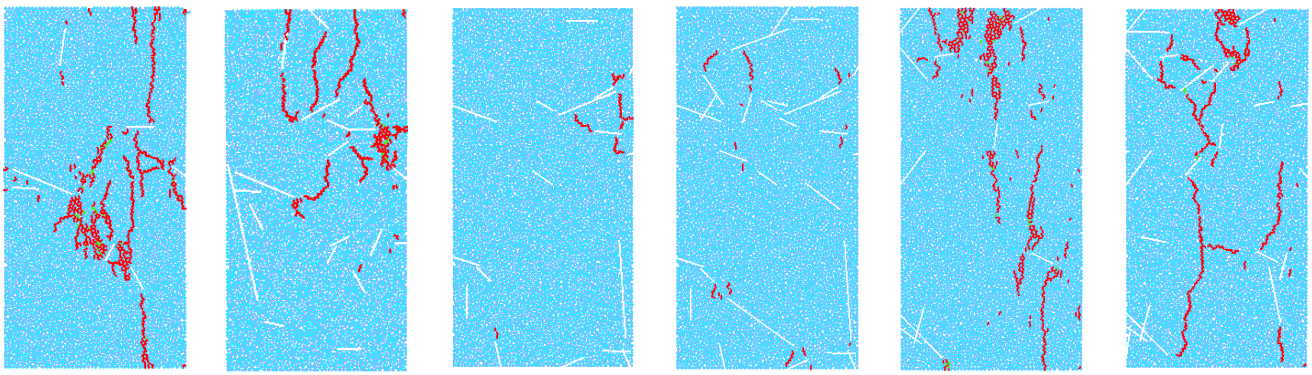

(a) #1_Aa (b) #2_Aa (c) #1_Ba (d) #2_Ba (e) #1_Ca (f) #2_Ca

Fig. 9 Damage of standard-scale rock specimen with different sampling methods in two SRMs. The white cracks of the specimens represent the initial joints or fractures in SRMs and the red and green cracks represent the new generated tension cracks and shear cracks under uniaxial compression

different (e.g., the UCS and E of rock specimens #2_Aa, #2_Ba, #2_Ca are 16.17 MPa, 6.22 MPa, 16.64 MPa and 7.95 GPa, 4.95 GPa, 9.23 GPa). The root of this phenomenon lies in the different sampling positions, which results in different initial cracks in the standard rock samples (as shown in Fig. 9), and different distribution of cracks leads to different mechanical properties of rocks.

The damage of standard-scale of rock specimen with different sampling methods in two SRMs are shown in Fig. 9. Note the white cracks of the specimens represents the initial joints or fractures in SRMs and the red and green cracks represent the new generated tension cracks and shear cracks under uniaxial compression. The failure modes are recorded at the time when residual strength is 80% of UCS by FISH language. It can be seen that the failure modes and damage degree (number of new cracks) of rock specimens

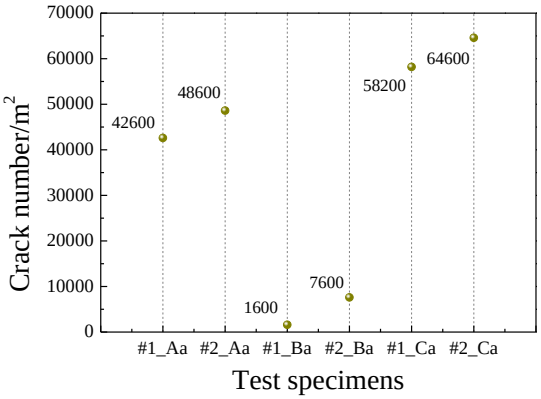

Fig. 10 Number of cracks per unit area at UCS of standard-scale rock specimens

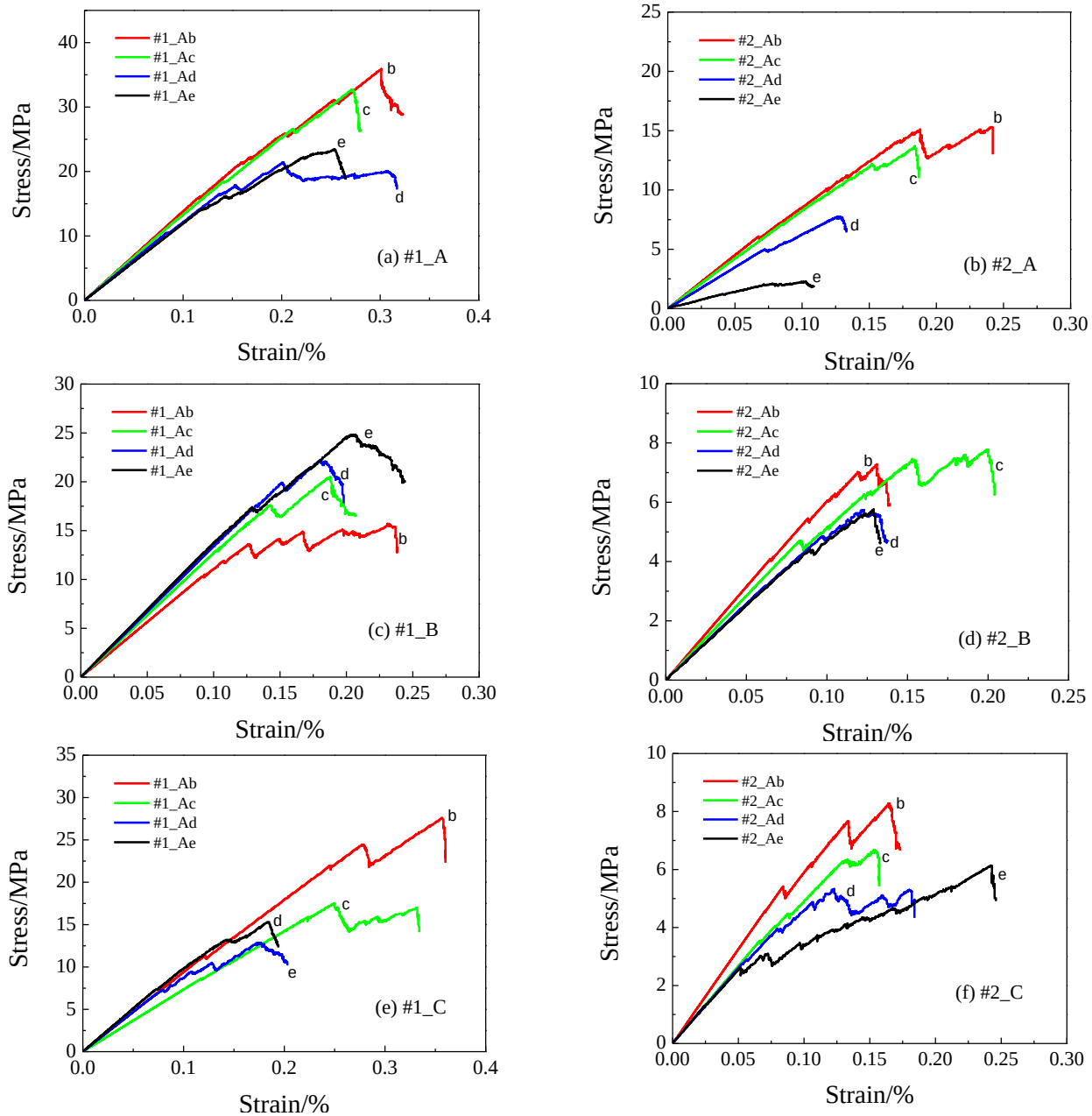

Fig. 11 Stress-strain curves of rock specimen with different scales. The scale of specimens b, c, d and e are 75 mm × 150 mm, 100 mm × 200 mm, 125 mm × 250 mm and 150 mm × 300 mm, respectively

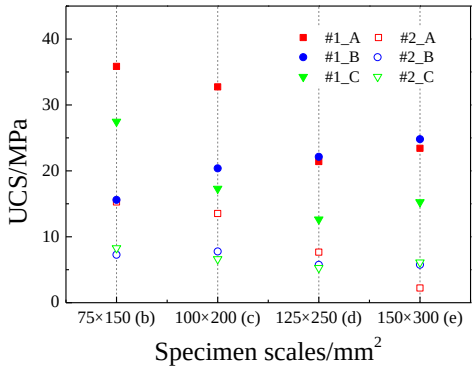

Fig. 12 UCS of differently scaled rock specimens

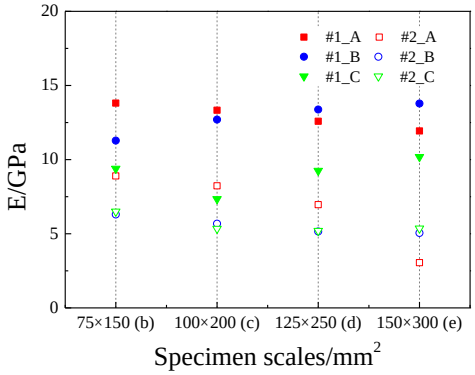

Fig. 13 E of rock specimen with different scales

with the different sampling method in two SRMs are different and the failure modes and degree of these specimens are controlled by tension cracks (red cracks).

The damage degree (number of new cracks) of rock specimens with sampling method A and C are larger than that of sampling method B. The reason is that the rock specimens obtained by the sampling method B contain more initial cracks, such as the initial crack of specimen #1_Ba is 18, larger than that of the specimens #1_Aa (7) and #1_Ca (11), which are more conducive fracture penetration. For the same sampling method, the damage degree (number of new cracks) of rock specimens sampling in SRM #1 are larger than sampling in SRM #2 due to SRM #2 containing more cracks for penetration.

Fig. 10 represent the number of cracks per unit area at UCS of standard-scale rock specimens. It can be seen from the graph that the change rule of the number of cracks per unit area at USC is opposite to that of UCS of rock specimen with different sampling methods in two SRMs. For instance, the UCS of SRM #1_Aa (32.79 MPa) are larger than SRM #2_Aa (16.17 MPa), while the number of cracks per unit area at UCS of SRM #1_Aa (42600) are less than SRM #2_Aa (48600). This shows that the strength of rock specimens with more new cracks is not necessarily less than that of rock specimens with fewer new cracks. The failure of rock is caused by the formation of macro-fracture surface.

4.2 Mechanical properties of jointed rock specimens with different scales

Figs. 11, 12 and 13 present the stress-strain curves, UCS and E of differently scaled rock specimens, respectively. Among them, the scale of specimens b, c, d and e are 75 mm × 150 mm, 100 mm × 200 mm, 125 mm × 250 mm and 150 mm × 300 mm, respectively. From these figures, it can be seen that the mechanical properties of rock specimens obtained by different sampling methods in SRM #1 and SRM #2 have different scale effects. With the increase of scale, the UCS of some rock specimens decreases first and then increases, such as #1_A (the UCS of the specimens b, c, d, e are 35.85 MPa, 32.7 MPa, 21.41 MPa, and 23.42 MPa), #1_C (the UCS of the specimens b, c, d, e are 27.46 MPa, 17.30 MPa, 12.63 MPa, and 15.25 MPa), and #2_C (the UCS of the specimens b, c, d, e are 8.27 MPa, 6.61 MPa, 5.27 MPa, and 6.11 MPa); the UCS of some rock specimens increases, such as #1_B (the UCS of the specimens b, c, d, e are 11.28 MPa, 12.70 MPa, 13.3 8 MPa, and 13.78 MPa); the UCS of some rock specimens decreases, such as #2_A (the UCS of the specimens b, c, d, e are 8.90 MPa, 8.23 MPa, 6.96 MPa, and 3.05 MPa); and the UCS of some rock specimens increases first and then decreases, such as #2_B (the UCS of the specimens b, c, d, e are 7.22 MPa, 7.77 MPa, 5.74 MPa, and 5.73 MPa).

As for elastic modulus E, with the increase of scale, some rock specimens show a decrease trend, such as #1_A (the E of the specimens b, c, d, e are 13.81 GPa, 13.33 GPa, 12.59 GPa, and 11.93 GP), #2_A (the E of the specimens b, c, d, e are 8.9 GPa, 8.23 GPa, 6.96 GPa, and 3.05 GP), #2_B (the E of the specimens b, c, d, e are 6.30 GPa, 5.68 GPa, 5.15 GPa, and 5.05 GP); some rock specimens show an increase trend, such as #1_B (the E of the specimens b, c, d, e are 11.28 GPa, 12.70 GPa, 13.38 GPa,

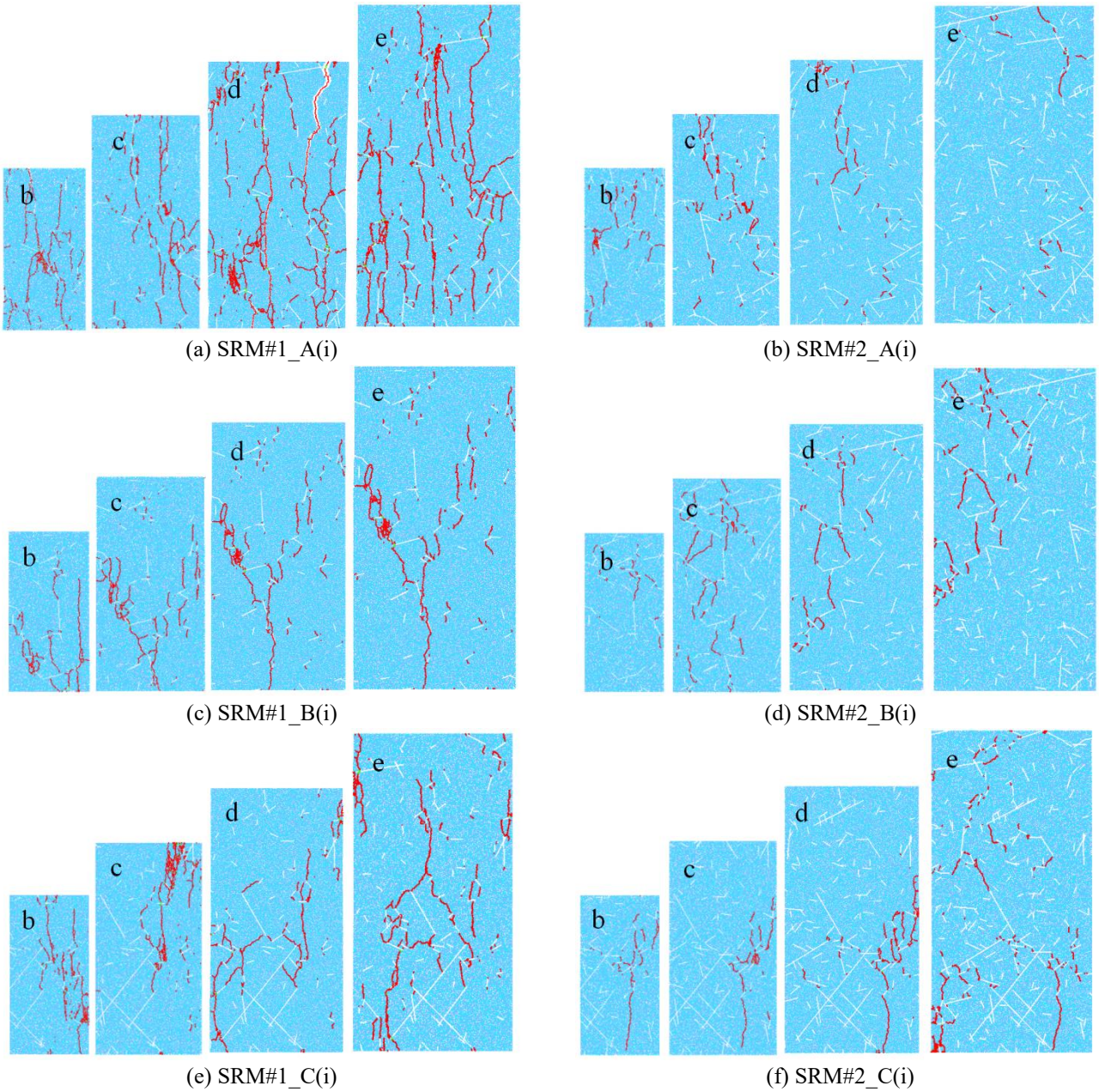

(a) SRM#1_A(i) (b) SRM#2_A(i)

(c) SRM#1_B(i) (d) SRM#2_B(i)

(e) SRM#1_C(i) (f) SRM#2_C(i)

Fig. 14 Damage of differently scaled rock specimens. i=b, c, d, e, represent different scaled rock specimens and the scales of rock specimens b, c, d, e are 75 mm × 150 mm, 100 mm × 200 mm, 125 mm × 250 mm and 150 mm × 300 mm

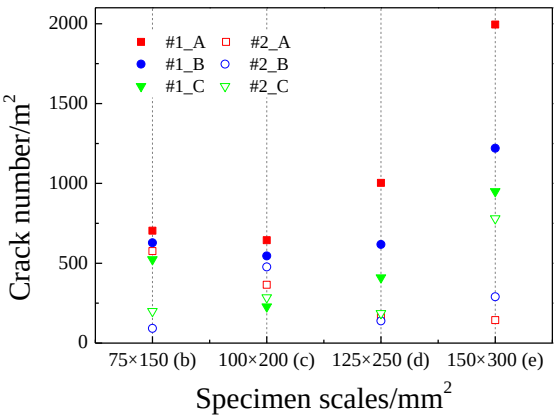

Fig. 15 Number of cracks per unit area at UCS of differently scaled rock specimens

and 13.78GPa); while some rock specimens show the trend of decreasing firstly and then increasing, such as #1_C (the E of the specimens b, c, d, e are 9.39 GPa, 7.34 GPa, 9.25 GPa, and 10.18 GP) and #2_C (the E of the specimens b, c, d, e are 6.50 GPa, 5.34 GPa, 5.20 GPa, and 5.36 GP). The reason of the difference of UCS and E of different rock specimens is that they have different distributions and scales of joints and fissures. The distributions and scales of joints and fissures are the root of the discreteness of rock mechanics.

The damage of differently scaled rock specimens is shown in Fig. 14. Obviously, due to the density of joint is different (SRM #2 is larger than SRM #1), the damage degree (number of new cracks) of rock specimens taken from SRM #1 is larger than that of rock specimens taken from SRM #2. The number of cracks produced by sampling method A is the largest, and the number of cracks produced by sampling method B and C are similarly when sampling at SRM #1. However, the number of cracks produced by sampling method A, B and C are similarly when sampling at SRM #2.

Fig. 15 presents the number of cracks per unit area at UCS of differently scaled rock specimens. With the increase of scale, the number of cracks per unit area at UCS of some rock specimens decreases first and then increases, such as #1_A (the cracks per unit area of the specimens b, c, d, e are 62578, 32200, 32096 and 44333), #1_B (the cracks per unit area of the specimens b, c, d, e are 55822, 27300, 18776 and 27111) and #1_C (the cracks per unit area of the specimens b, c, d, e are 46577, 11400, 13120 and 21111); some rock specimens show a decrease trend, such as #2_A (the cracks per unit area of the specimens b, c, d, e are 51200, 18350, 5216 and 3200); and some rock specimens show a trend of increase-decrease-increase-decrease, such as #2_B (the cracks per unit area of the specimens b, c, d, e are 8178, 23850, 4448 and 6444) and #2_C (the cracks per unit area of the specimens b, c, d, e are 17689, 14250, 5952 and 17333). This further illustrates that the failure of rock is caused by the formation of macro-fracture surface.

5. Conclusions

In this paper, two synthetic rock mass (SRM #1 and SRM #2) were established by PB model and smooth-joint model firstly, then three sampling methods (A, B, C) were used to sampling different scaled rock specimens. Finally, the mechanical properties and failure modes of different rock specimens were discussed. Some meaningful conclusions are drawn as follow.

The smaller the initial fracture density is, the greater the UCS and E is when compared with the same sampling location. Meanwhile, the UCS and E of rock specimens with different sampling method in same SRM are different.

The mechanical properties of rock specimens obtained by different sampling methods in different SRMs have different scale effects. With the increase of rock scale, the change of UCS and E of rock specimens shows different trends, some rock specimens may have a trend of decrease-increase, increase, decrease, increase- decrease, etc., and this trend are determined by the number and the distribution of cracks.

The number of new cracks of rock specimens with sampling in SRM with a lower fracture density is larger than that sampling in SRM with a higher fracture density. The strength of rock specimens with more new cracks is not necessarily less than that of rock specimens with fewer new cracks and the failure of rock is caused by the formation of macro-fracture surface.

Acknowledgments

This research is supported by the Postgraduate Research & Practice Innovation Program of Jiangsu Province (No. KYCX19-0094).

References

Bahaaddini, M., Sharrock, G. and Hebblewhite, B.K. (2013), "Numerical investigation of the effect of joint geometrical parameters on the mechanical properties of a non-persistent jointed rock mass under uniaxial compression", *Comput. Geotech.*, **49**, 206-225. https://doi.org/10.1016/j.compgeo.2012.10.012.

Bahrani, N. and Kaiser, P.K. (2016), "Numerical investigation of the influence of specimen size on the unconfined strength of defected rocks", *Comput. Geotech.*, **77**, 56-67. https://doi.org/10.1016/j.compgeo.2016.04.004.

Itasca Consulting Group Inc. (2014), "PFC (particle flow code), version 5.0". ICG, Minneapolis, Minnesota, U.S.A., http://www.itascacg.com/software/pfc.

Kim, J.S., Kim, G.Y., Baik, M.H. and Cho, G.C. (2019), "A new approach for quantitative damage assessment of in-situ rock mass by acoustic emission", *Geomech. Eng.*, **18**(1), 11-20. https://doi.org/10.12989/gae.2019.18.1.011.

Lee, H. and Jeon, S. (2011), "An experimental and numerical study of fracture coalescence in pre-cracked specimens under uniaxial compression", *Int. J. Solids Struct.*, **48**(6), 979-999. https://doi.org/10.1016/j.ijsolstr.2010.12.001.

Morris, J.P., Rubin, M.B., Block, G.I. and Bonner, M.P. (2006), "Simulations of fracture and fragmentation of geologic materials using combined FEM/DEM analysis", *Int. J. Impact Eng.*, **33**(1-12), 463-473. https://doi.org/10.1016/j.ijimpeng.2006.09.006.

Potyondy, D.O. (2015), "The bonded-particle model as a tool for rock mechanics research and application: Current trends and future directions", *Geosyst. Eng.*, **18**(1), 1-28. https://doi.org/10.1080/12269328.2014.998346.

Shemirani, A.B., Haeri, H., Sarfarazi, V. and Hedayat, A. (2017), "A review paper about experimental investigations on failure behaviour of non-persistent joint", *Geomech. Eng.*, **13**(4), 535-570. https://doi.org/10.12989/gae.2017.13.4.535.

Singh, M. and Rao, K.S. (2005), "Empirical methods to estimate the strength of jointed rock masses", *Eng. Geol.*, **77**(1-2), 127-137. https://doi.org/10.1016/j.enggeo.2004.09.001.

Song, H., Jiang, Y., Elsworth, D., Zhao, Y.X., Wang, J.H. and Liu, B. (2018), "Scale effects and strength anisotropy in coal", *Int. J. Coal Geol.*, **195**, 37-46. https://doi.org/10.1016/j.coal.2018.05.006.

Symons, I.F. (1970), "The effect of size and shape of specimen upon the unconfined compressive strength of cement-stabilized materials", *Mag. Concrete Res.*, **22**(70), 45-51. https://doi.org/10.1680/macr.1970.22.70.45.

Toraño, J., Díez, R.R., Cid, J.M.R. and Barciella, M.M.C. (2002),

"FEM modeling of roadways driven in a fractured rock mass under a longwall influence", *Comput. Geotech.*, **29**(6), 411-431. https://doi.org/10.1016/S0266-352X(02)00006-X.

Wang, P., Cai, M., Ren, F., Li, C.H. and Yang, T.H. (2017), "A digital image-based discrete fracture network model and its numerical investigation of direct shear tests", *Rock Mech. Rock Eng.*, **50**(7), 1801-1816. https://doi.org/10.1007/s00603-017-1200-8.

Wang, X. and Tian, L. (2018), "Mechanical and crack evolution characteristics of coal-rock under different fracture-hole conditions: A numerical study based on particle flow code", *Environ. Earth Sci.*, **77**(8), 297. https://doi.org/10.1007/s12665-018-7486-3.

Wong, R.H.C. and Chau, K.T. (1998), "Crack coalescence in a rock-like material containing two cracks", *Int. J. Rock Mech. Min. Sci.*, **35**(2), 147-164. https://doi.org/10.1016/S0148-9062(97)00303-3.

Wu, N., Liang, Z., Zhou, J. and Zhang, Y. (2020), "Energy evolution characteristics of coal specimens with preformed holes under uniaxial compression", *Geomech. Eng.*, **20**(1), 55-66. https://doi.org/10.12989/gae.2019.18. 6.627.

Xi, Y., Jun, L., Zeng, Y. and Jiang, T. (2018), "Research on lateral scale effect and constitutive model of rock damage energy evolution", *Geotech. Geol. Eng.*, **36**(4), 2415-2424. https://doi.org/10.1007/s10706-018-0473-3.

Zhang, Q., Wang, X., Tian, L. and Huang, D.M. (2018), "Analysis of mechanical and acoustic emission characteristics of rock materials with double-hole defects based on particle flow code", *Shock Vib.*, 7065029. https://doi.org/10.1155/2018/7065029.

CC